scientific reports

OPEN

Impact of pre-annealing process on electrical properties and stability of indium zinc oxide thin-film transistors

Han-Lin Zhao[1], Gergely Tarsoly[1], Fei Shan[1], Xiao-Lin Wang[1], Jae-Yun Lee[1], Yong Jin Jeong[2] & Sung-Jin Kim[1]✉

This paper examined the effects of no treatment versus plasma treatment, and femtosecond laser irradiation as pre-annealing processes on indium zinc oxide (IZO) films and annealing at high temperatures. The plasma pre-annealed multilayer stacked IZO TFTs showed better electrical properties with mobility enhancement from 2.45 to 7.81 cm^2/Vs, but exhibited diminished on–off current ratio (I_{on}/I_{off}). The IZO thin-film transistor (TFT) prepared with femtosecond laser pre-annealing with low pulse energy generation (power of 3 W at 700 nm wavelength) for 100 s has also exhibited significantly improved electrical performance, the saturation mobility increased to 4.91 cm^2/Vs, the I_{on}/I_{off} ratio was enhanced from 4.5×10^5 to 2.1×10^6, the threshold voltage improved from − 1.44 to − 0.25 V, and the subthreshold swing was reduced from 1.21 to 0.61 V/dec. In conclusion, IZO TFTs with improved performance can be prepared using a femtosecond laser pre-annealing process, which has great potential for fabricating low-cost, high-performance devices.

Amorphous metal oxide semiconductors have been studied extensively for the development of thin-film transistors (TFTs) because of their applicability in wearable electronic circuits, favorable optical transparency in the visible region, and reduced fabrication costs through low-temperature processes. Indium oxide, indium zinc oxide (IZO), indium gallium zinc oxide, and several other metal oxides have been utilized[1–6].

IZO is one of the widely used active layer materials for TFTs because of its wide bandgap (3.68–3.76 eV), high mobility, high transparency, and smooth surface[7–10]. Multi-stacked IZO layers have lower porosity and higher density than single layers and can generate more electron carriers and exhibit improved electrical properties. Multi-stacked IZO films need to be annealed several times during preparation to obtain high-density films[11,12]. Multi-stacked IZO TFTs can be fabricated using solution processes, vacuum evaporation, chemical vapor deposition, and atomic layer deposition techniques. Of these, solution processes have the advantages of simple fabrication, low-temperature processing, and low cost[13–19]. In addition, oxygen (O_2) plasma treatment, photochemical activation, femtosecond laser treatment, and thermal annealing under an O_2 atmosphere were shown to improve the surface quality of the films and enhance the electrical properties of multi-stacked IZO TFTs[20–22]. The plasma pre-annealing treatment at low power (< 150 W) was demonstrated to improve the electrical properties of oxide TFTs by reducing the charge carrier concentration and conductivity, and offers the advantages of low cost, high efficiency, and large area uniformity[23,24]. A pre-annealing process using femtosecond lasers applies the laser to a specific spot of the film, resulting in less thermal damage in the film through which the laser passes. Femtosecond laser technology is used widely for TFT preparation because of its relatively short laser pulses and high transient intensity, which reduces the cost and avoids damage to oxide films[25,26].

In this study, TFTs composed of IZO films treated with different pre-annealing processes of plasma and femtosecond laser were fabricated to achieve high mobility and relatively good electrical stability and provide a relatively simple, low-cost preparation method. In addition, the effects of different pre-annealing processes on IZO TFTs were compared.

[1]College of Electrical and Computer Engineering, Chungbuk National University, Cheongju 28644, Korea. [2]Department of Materials Science and Engineering, Korea National University of Transportation, Chungju 27469, Republic of Korea. ✉email: ksj@cbnu.ac.kr

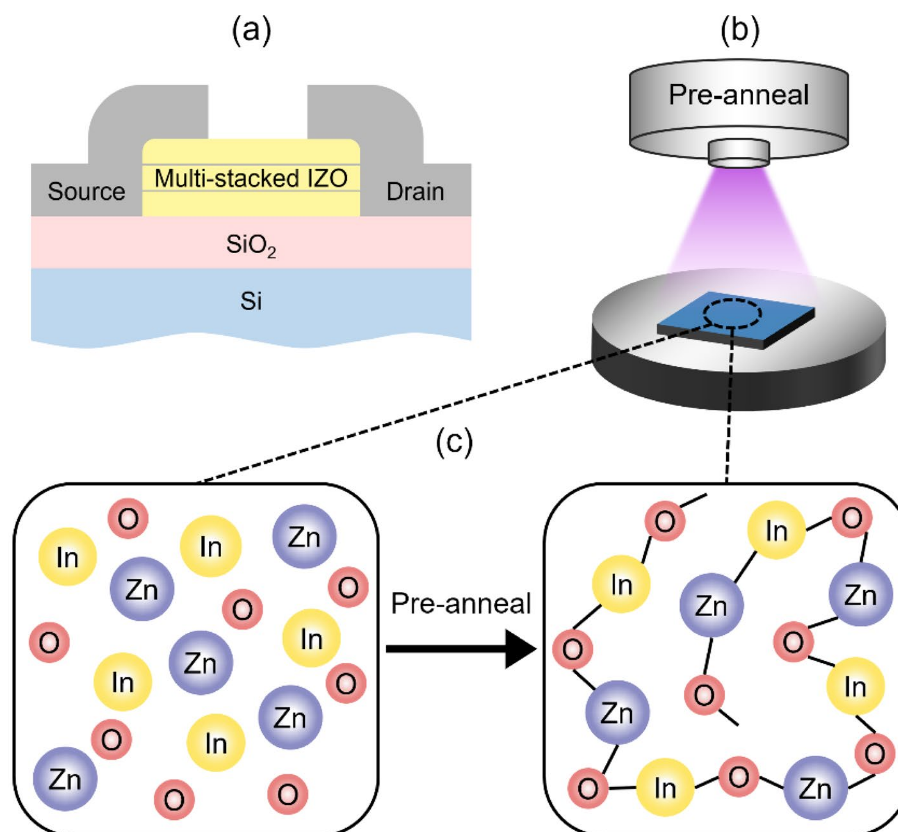

Figure 1. (**a**) Schematic diagram of the device fabrication process for multi-stacked IZO TFTs. Sketches of (**b**) plasma and (**c**) femtosecond laser pre-annealing.

Experimental details

A multi-stacked IZO film was manufactured on the a heavily dopped n-type Silicon bottom gate substrate that has a hot-grown 100 nm thick Silicon dioxide layer used a dielectric layer, as shown in Fig. 1a. First, the substrate was cleaned with piranha solution (3:1 ratio of sulfuric acid to hydrogen peroxide) at 80 °C, sonicated sequentially in DI water, acetone, and isopropanol for 20 min each at 45 °C, and blow dried with nitrogen gas. All residual solvent was removed by drying the samples in an oven at 60 °C for 30 min.

2.5 ml of a 0.1 M precursor solution of indium nitrate hydrate [$In(NO_3)_3 \cdot xH_2O$] in 2-methoxyethanol was prepared in a glass vial, and 50 µl of acetylacetone, and 22.5 µl of ammonia were added. Subsequently, 1.5 ml of a 0.1 M zinc acetate dihydrate [$Zn(CH_3COO)_2 \cdot 2H_2O$] solution in 2-methoxyethanol was prepared, and 30 µl acetylacetone was added. Both solutions were placed in a magnetic stirrer at 700 rpm and stirred at 60 °C for 1 h. The two solutions were mixed at a 1:1 ratio and stirred at 500 rpm and room temperature for 2 h to prepare the IZO precursor solution. The mixed solution was filtered through a 0.2 µm syringe filter to remove particulates and to obtain a more transparent and homogeneous solution, which is beneficial for spin-coating. The precursor solution was spin-coated on four clean silicon substrates at 1,500 rpm for 30 s, followed by a 30 min annealing process at 400 °C. This resulted in an IZO thickness of 20 nm. The same spin-coating and annealing processes were repeated to form the second layer. For forming the third layer, the spin-coating process under the same conditions was repeated again, but with different pre-annealing conditions. To fabricate the devices with plasma treated layers, the IZO layer was treated with oxygen plasma at an RF power level of 150 W for 3 min (with the schematics shown in Fig. 1b], where the plasma produced a uniform O_2^+/e^- radiation over an appropriate area, transforming from O_2 at 3 sccm. For the laser irradiated IZO films, an ultrashort pulse mode-locked titanium:sapphire femtosecond laser system (Coherent, Chameleon Ultra II) generated at low pulse energy with a power of 3 W and a 700 nm wavelength was used for 100 s. The schematics of the effect of pre-annealing is shown in Fig. 1c. For control, samples with neither laser nor oxygen plasma pre-annealing treatment were also prepared. All devices (treated and untreated) were hard baked for 1 h at 400 °C, and then cooled back to room temperature. The 100 nm thick aluminum source and drain electrodes were deposited on top of the IZO films by thermal evaporation (pressure ~ 10 – 6 Torr, rate 0.1 Å/s) through the same shadow mask with a channel width of 2000 µm and a length of 200 µm.

The surface morphology and properties of multi-stacked IZO films were analyzed by atomic force microscopy (AFM) and X-ray photoelectron spectroscopy (XPS). The electrical characteristics of the output, transfer, and stability of the TFTs were measured using a semiconductor parameter analyzer (Keithley 4200, Keithley Instruments LLC, Cleveland, Ohio) in a dark room at room temperature.

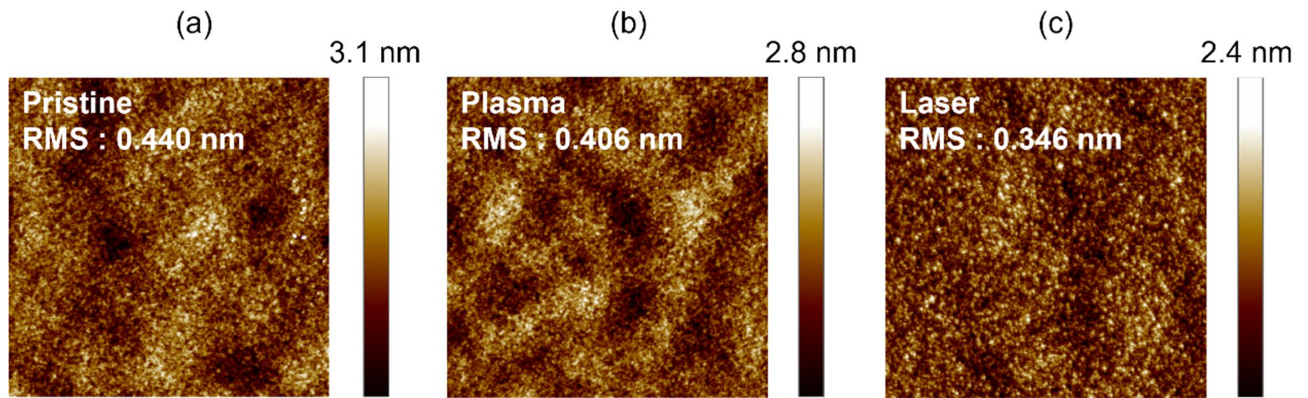

Figure 2. AFM images of multi-stacked IZO thin-film surfaces under (**a**) pristine, (**b**) plasma, and (**c**) femtosecond laser pre-annealing.

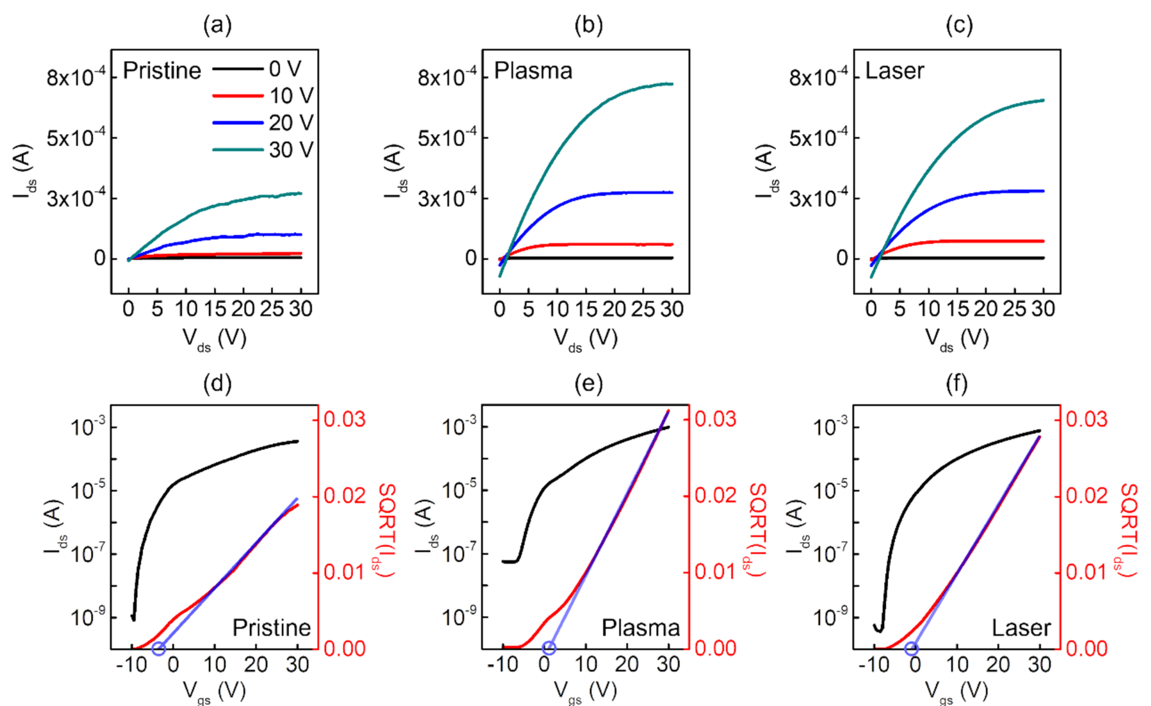

Figure 3. Output characteristics of multi-stacked IZO TFTs with (**a**) pristine, (**b**) plasma, and (**c**) femtosecond laser pre-annealing. Transfer characteristics and SQRT transfer curves of multi-stack IZO TFTs with (**d**) pristine, (**e**) plasma, and (**f**) femtosecond laser pre-annealing.

Results and discussion

The surface morphology of the multi-stacked IZO films treated with different pre-annealing methods was analyzed by AFM; Fig. 2a–c show the corresponding height distribution of each AFM image. The root mean square (RMS) roughness of pristine, plasma, and femtosecond laser pre-annealed IZO films was 0.440, 0.406, and 0.346 nm, respectively. From the cross-sectional image, plasma pre-annealing positively affects the surface roughness of the multi-stacked IZO films. The film surface was smoother and more uniform than the pristine sample. The IZO films irradiated with femtosecond laser pre-annealing showed a more uniform granular structure, and the deposited films showed a continuous and smooth surface with no obvious wave crests. The roughness may contribute to the leakage currents, which deteriorate the electrical properties (e.g., electron mobility) of the device[27,28]. This suggests that a proper pre-annealing process involving plasma or femtosecond laser treatments can lead to more homogeneous multi-stacked IZO films.

Figure 3a–c show the output characteristic curves of the drain current (I_{ds}) at constant gate bias voltages (V_{gs}) of 0, 10, 20, and 30 V, drain bias voltage (V_{ds}) incremented from 0 to 30 V in 10 V increments to investigate the electrical characteristics of the trhee types of IZO TFTs. All devices exhibited typical *n*-type output characteristics, but the one with femtosecond laser and plasma treated IZO had smoother and more stable saturation curves than the other IZO TFTs. On the other hand, the femtosecond laser and plasma treated IZO TFTs showed leakage

Treatment methods	μ_{sat} (cm^2/Vs)	I_{on}/I_{off}	V_{th} (V)	SS (V/dec)	N_{it} ($\times 10^{12}$ cm^{-2})
Pristine	2.45	4.4×10^5	− 1.44	1.21	5.98 ± 0.43
Plasma	7.81	1.8×10^4	1.13	0.68	3.94 ± 0.96
Laser	4.91	2.1×10^6	− 0.25	0.61	2.53 ± 0.29

Table 1. Electrical performance of multi-stack IZO TFTs with pristine, plasma, and laser pre-annealing.

currents at low drain voltages. Figure 3d–f shows the transfer curves, and square root (SQRT) transfer curves of the pristine, plasma, and femtosecond laser pre-annealing treated TFTs when the bias voltage was applied with V_{ds} fixed at 30 V as V_{gs} was increased from − 10 V to 30 V in 0.5 V increments. All the TFTs showed typical n-type characteristics as I_{ds} increased with V_{gs} and exhibited a significant transition from the off-state to the on-state.

For comparison, Table 1 lists the saturation mobility (μ_{sat}), threshold voltage (V_{th}), on/off current ratios (I_{on}/I_{off}), and subthreshold swing (SS) values of the pristine, plasma, and femtosecond laser pre-annealed multi-stacked IZO TFTs. Compared to the device with pristine IZO, which had a mobility of μ_{sat} = 2.45 cm^2/Vs, the devices with plasma treatment had higher electron mobility (μ_{sat} = 7.81 cm^2/Vs).The ones with the femtosecond laser treatment also showed improved performance (μ_{sat} = 4.91 cm^2/Vs). On the other hand, the I_{on}/I_{off} of the plasma-treated IZO TFT decreased compared to the pristine one, with V_{th} shifting from − 1.44 V to 1.13 V in the positive direction. By contrast, the femtosecond laser treatment resulted in an increase in I_{on}/I_{off} to 2.1×10^6, and an improved V_{th} shift to − 0.25 V. Significant improvements in the SS values were also observed for both pre-annealed IZO TFTs, particularly for the femtosecond laser-treated ones, from the 1.21 V/dec of the pristine device to 0.61 V/dec. The improved electrical properties of the devices correlated with the lower SS values, which relate to the interfacial trap density (N_{it}), as expressed in Eq. (1),

$$N_{it} = \frac{C_i}{q}\left[\frac{SS\log(e)}{kT/q} - 1\right], \tag{1}$$

where C_i is the accumulation capacitance of an insulator per unit area; q is the electron charge, k is the Boltzmann's constant, and T is the temperature. The calculated N_{it} values of the pristine, plasma, and femtosecond laser-treated multi-stacked IZO TFTs were 5.98 ± 0.43, 3.94 ± 0.96, and 2.53 ± 0.29 ($\times 10^{12}$ cm^{-2}), respectively (Fig. 4a). The interfacial trapping density is closely related to the SS, and a decrease in the SS value signifies a decrease in the number of traps at the interface[29,30]. The use of femtosecond laser results in the smallest number of interface trap states among the three types of devices, resulting in better overall electrical performance when measuring the characteristics of multilayer IZO TFTs.

The bias stress stability characteristics of the pristine, plasma, and femtosecond laser-treated TFTs were measured. The time evolution of I_{ds} measured in the TFTs normalized to the initial value with a duration of 600 s and V_{gs} and V_{ds} both biased at 30 V (on state), as shown in Fig. 4b. The decrease in current with stress time was evident, with an initial rapid decrease followed by a prolonged and slow decrease without establishing a steady state. This behavior is consistent with a shift in the device V_{th} caused by charge trapping[31]. The pristine IZO surface exhibited the highest attenuation of the drain current due to the presence of many defects, with the normalized I_{ds} dropping to a final value of 0.77 after 600 s. The normalized I_{ds} of the plasma treated devices has dropped to 0.69, and for the femtosecond laser one it decreased to 0.77 during the same time interval. The femtosecond laser irradiated devices show improved stability. On the long term, the device may deteriorate due to environmental factors such as water, oxygen, etc. Measuring the device performance 10 days after the fabrication, for the pristine device, a tenfold increase in the off curent was observed, but other parts of the transfer curve has remained relatively unchanged, as shown in Fig. 4c. For the devices with either plasma or laser pre-annealing treatment, there is no significant change in the transfer curves. These results demonstrate that the pre-annealing treatments have some passivation effect on semiconductor thin film.

The effect of oxygen content of the IZO films on the electrical properties of the devices was studied. The multilayer structured IZO films were examined by XPS to determine the effects of pre-annealing methods of plasma and femtosecond laser treatment on the IZO films compared to the pristine sample device, as shown in Fig. 5a. The O 1s peak was fitted by three near-Gaussian curves centered at 530.1 (O_1), 531.2 (O_2), and 532.4 (O_3) eV, which were assigned to metal-bonded oxygen (M–O), oxygen vacancies (O_V), and hydroxide species (O–H), respectively. Figure 5b shows the O 1s area ratios of the three Gaussians. The plasma pre-annealed IZO films had a higher O_V peak area, but the area of M–O peak decreased. O_V is generally considered to be a shallow donor that is formed by the breakage of In–O and Zn–O bonds. Compared to the pristine IZO TFTs, the oxygen atmosphere in plasma pre-annealing promoted the decomposition of M–O, increasing the O_V and improving the carrier concentration, and affecting the associated mobility. The relative area of the M–O lattice peaks of the femtosecond laser pre-annealed films were reduced relative to the original, and the area of the O_V peaks was increased[25,32]. The variation of the electrical properties is consistent with the trends in Table 1 and Fig. 5b. The proportion of O–H groups was similar, resulting in a minor effect on the electrical performance.

Conclusion

The effects of plasma, and femtosecond laser pre-annealing processes on the performance of multi-stacked IZO-based devices were studied by comparing the characteristics to devices with pristine multi-stack IZO active layers. The plasma pre-annealed multi-stacked IZO TFTs showed improved electrical properties with a mobility of 7.81 cm^2/Vs. The optimized preparation process for the femtosecond laser pre-annealed IZO TFTs was demonstrated,

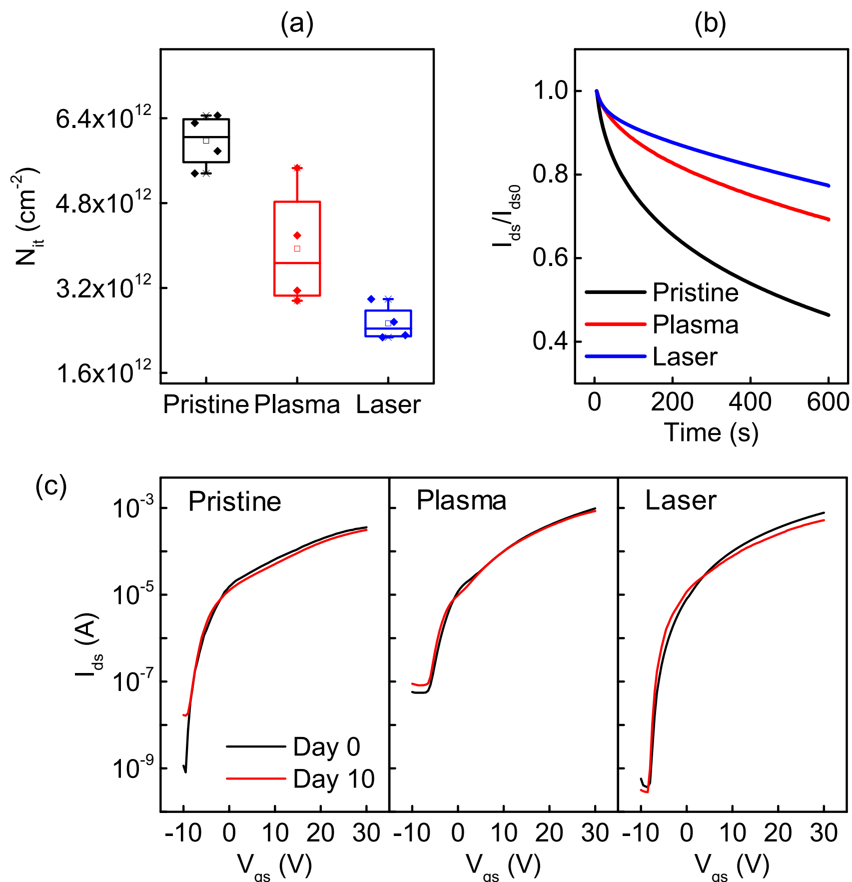

Figure 4. Multi-stacked IZO TFTs (**a**) interface trap charges, (**b**) stress time stability characteristics in pristine, plasma, and femtosecond laser pre-annealing and (**c**) transfer curves of devices compared after 10 days of storage under ambient conditions.

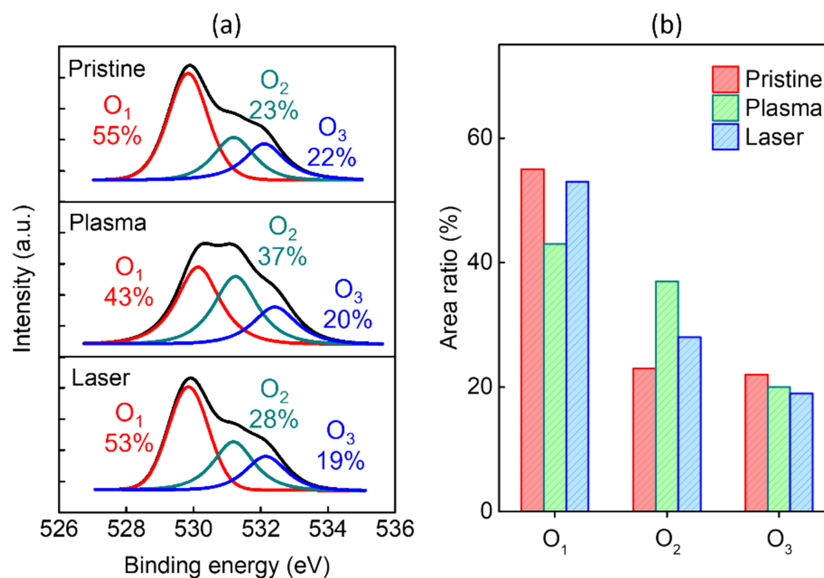

Figure 5. (**a**) XPS O 1s analysis of multi-stacked IZO films with pristine, plasma, and femtosecond laser pre-annealing. (**b**) Analytical areas of O1 peaks for M–O lattices, O_V states, and O–H species based on different pre-annealing processes of pristine, plasma, femtosecond laser.

showing an improved I_{on}/I_{off} enhancement to 2.1×10^6. Femtosecond laser pre-annealing has important theoretical and practical implications for improving the electrical properties and time stress stability of oxide IZO TFTs for the low-cost fabrication of amorphous oxide electronics.

Data availability

The dataset used and/or analyzed during the current study available from the corresponding author on reasonable request.

Received: 24 August 2022; Accepted: 9 November 2022
Published online: 14 November 2022

References

1. Nomura, K. *et al.* Room-temperature fabrication of transparent flexible thin-film transistors using amorphous oxide semiconductors. *Nature* **432**, 488–492 (2004).
2. Fortunato, E., Barquinha, P. & Martins, R. Oxide semiconductor thin-film transistors: A review of recent advances. *Adv. Mater.* **24**, 2945–2986 (2012).
3. Sabri, M. M. *et al.* Hydroxyl radical-assisted decomposition and oxidation in solution-processed indium oxide thin-film transistors. *J. Mater. Chem. C.* **3**, 7499–7505 (2015).
4. Han, S.-Y., Herman, G. S. & Chang, C.-H. Low-temperature, high-performance, solution-processed indium oxide thin-film transistors. *J. Am. Chem. Soc.* **133**, 5166–5169 (2011).
5. Seo, J.-S. & Bae, B.-S. Improved electrical performance and bias stability of solution-processed active bilayer structure of indium zinc oxide based TFT. *ACS Appl. Mater. Interfaces* **6**, 15335–15343 (2014).
6. Hoshino, K., Hong, D., Chiang, H. Q. & Wager, J. F. Constant-voltage-bias stress testing of a-IGZO thin-film transistors. *IEEE Trans. Electron Devices* **56**, 1365–1370 (2009).
7. Morales-Masis, M., De Nicolas, S. M., Holovsky, J., De Wolf, S. & Ballif, C. Low-temperature high-mobility amorphous IZO for silicon heterojunction solar cells. *IEEE J. Photovolt.* **5**, 1340–1347 (2015).
8. Paine, D. C., Yaglioglu, B., Beiley, Z. & Lee, S. Amorphous IZO-based transparent thin film transistors. *Thin Solid Films* **516**, 5894–5898 (2008).
9. Koo, C. Y. *et al.* Low temperature solution-processed InZnO thin-film transistors. *J. Electrochem. Soc.* **157**, J111 (2010).
10. Martins, R. *et al.* Write-erase and read paper memory transistor. *Appl. Phys. Lett.* **93**, 203501 (2008).
11. Kim, D. J. *et al.* Improved electrical performance of an oxide thin-film transistor having multistacked active layers using a solution process. *ACS Appl. Mater. Interfaces* **4**, 4001–4005 (2012).
12. Hong, S., Park, J. W., Kim, H. J., Kim, Y.-G. & Kim, H. J. A review of multi-stacked active-layer structures for solution-processed oxide semiconductor thin-film transistors. *J. Inf. Disp.* **17**, 93–101 (2016).
13. Kim, G. H. *et al.* Formation mechanism of solution-processed nanocrystalline InGaZnO thin film as active channel layer in thin-film transistor. *J. Electrochem. Soc.* **156**, H7 (2008).
14. Kaleemulla, S., Reddy, A. S., Uthanna, S. & Reddy, P. S. Physical properties of In_2O_3 thin films prepared at various oxygen partial pressures. *J. Alloys Compd.* **479**, 589–593 (2009).
15. Jung, C. *et al.* Highly crystalline CVD-grown multilayer $MoSe_2$ thin film transistor for fast photodetector. *Sci. Rep.* **5**, 1–9 (2015).
16. Sheng, J., Park, E. J., Shong, B. & Park, J.-S. Atomic layer deposition of an indium gallium oxide thin film for thin-film transistor applications. *ACS Appl. Mater. Interfaces* **9**, 23934–23940 (2017).
17. Park, J. W., Kang, B. H. & Kim, H. J. A review of low-temperature solution-processed metal oxide thin-film transistors for flexible electronics. *Adv. Funct. Mater.* **30**, 1904632 (2020).
18. Liu, A. *et al.* Hole mobility modulation of solution-processed nickel oxide thin-film transistor based on high-k dielectric. *Appl. Phys. Lett.* **108**, 233506 (2016).
19. Kim, Y. G., Kim, T., Avis, C., Lee, S.-H. & Jang, J. Stable and high-performance indium oxide thin-film transistor by Ga doping. *IEEE Trans. Electron Devices* **63**, 1078–1084 (2016).
20. Mancinelli, A., Bolat, S., Kim, J., Romanyuk, Y. E. & Briand, D. Deep-UV-enhanced approach for low-temperature solution processing of IZO transistors with high-k AlO_x/$YAlO_x$ Dielectric. *ACS Appl. Mater. Interfaces* **2**, 3141–3151 (2020).
21. Carlos, E. *et al.* UV-mediated photochemical treatment for low-temperature oxide-based thin-film transistors. *ACS Appl. Mater. Interfaces* **8**, 31100–31108 (2016).
22. Qiang, L., Liang, X., Pei, Y., Yao, R. & Wang, G. Extraction method of trap densities for indium zinc oxide thin-film transistors processed by solution method. *Thin Solid Films* **649**, 51–56 (2018).
23. Shim, J. *et al.* High-performance 2D rhenium disulfide (ReS_2) transistors and photodetectors by oxygen plasma treatment. *Adv. Mater.* **28**, 6985–6992 (2016).
24. Ma, M.-W., Chiang, T.-Y., Wu, W.-C., Chao, T.-S. & Lei, T.-F. Characteristics of HfO_2/Poly-Si interfacial layer on CMOS LTPS-TFTs with HfO_2 gate dielectric and O_2 plasma surface treatment. *IEEE Trans. Electron Devices* **55**, 3489–3493 (2008).
25. Chen, C. *et al.* Solution-processed metal oxide arrays using femtosecond laser ablation and annealing for thin-film transistors. *J. Mater. Chem. C.* **5**, 9273–9280 (2017).
26. Lee, C. *et al.* Control of current saturation and threshold voltage shift in indium oxide nanowire transistors with femtosecond laser annealing. *ACS Nano* **5**, 1095–1101 (2011).
27. Sharma, A., Chourasia, N. K., Pal, N., Biring, S. & Pal, B. N. Role of electron donation of TiO_2 gate interface for developing solution-processed high-performance one-volt metal-oxide thin-film transistor using ion-conducting gate dielectric. *J. Phys. Chem. C.* **123**, 20278–20286 (2019).
28. Seul, H. J., Kim, H.-G., Park, M.-Y. & Jeong, J. K. A solution-processed silicon oxide gate dielectric prepared at a low temperature via ultraviolet irradiation for metal oxide transistors. *J. Mater. Chem. C.* **4**, 10486–10493 (2016).
29. Bukke, R. N. *et al.* Lanthanum doping in zinc oxide for highly reliable thin-film transistors on flexible substrates by spray pyrolysis. *ACS Appl. Mater. Interfaces* **12**, 35164–35174 (2020).
30. Saha, J. K., Bukke, R. N. & Jang, J. Extremely stable, high performance Gd and Li alloyed ZnO thin film transistor by spray pyrolysis. *Adv. Electron. Mater.* **6**, 2000594 (2020).
31. Kaftanoglu, K. *et al.* Stability of IZO and a-Si: H TFTs processed at low temperature (200 ℃). *J. Inf. Disp.* **7**, 339–343 (2011).
32. Luo, D. *et al.* Effects of etching residue on positive shift of threshold voltage in amorphous indium–zinc-oxide thin-film transistors based on back-channel-etch structure. *IEEE Trans. Electron Devices* **61**, 92–97 (2013).

Acknowledgements

This research was supported by the MSIT (Ministry of Science and ICT), Korea, under the Grand Information Technology Research Center support program (IITP-2022-2020-0-01462) supervised by the IITP (Institute

for Information & communications Technology Planning & Evaluation), and by the Basic Science Research Program through the National Research Foundation of Korea (NRF) funded by the Ministry of Education (No. 2020R1A6A1A12047945).

Author contributions

H.-L.Z.: Formal analysis, Validation, Visualization, Writing—original draft. F.S. and X.-L.W.: Data curation, Investigation, Visualization. J.-Y.L., G.T., and Y.J.J.: Investigation. S.-J.K.: Writing—review & editing, Supervision.

Competing interests

The authors declare no competing interests.

Additional information

Correspondence and requests for materials should be addressed to S.-J.K.

Reprints and permissions information is available at www.nature.com/reprints.

Publisher's note Springer Nature remains neutral with regard to jurisdictional claims in published maps and institutional affiliations.

Open Access This article is licensed under a Creative Commons Attribution 4.0 International License, which permits use, sharing, adaptation, distribution and reproduction in any medium or format, as long as you give appropriate credit to the original author(s) and the source, provide a link to the Creative Commons licence, and indicate if changes were made. The images or other third party material in this article are included in the article's Creative Commons licence, unless indicated otherwise in a credit line to the material. If material is not included in the article's Creative Commons licence and your intended use is not permitted by statutory regulation or exceeds the permitted use, you will need to obtain permission directly from the copyright holder. To view a copy of this licence, visit http://creativecommons.org/licenses/by/4.0/.

© The Author(s) 2022